

Imaging Flux Vortices in MgB₂ using Transmission Electron Microscopy

J.C. Loudon,¹ C.J. Bowell,^{1,*} N.D. Zhigadlo,² J. Karpinski,² and P.A. Midgley¹

¹*Department of Materials Science and Metallurgy, University of Cambridge, Pembroke Street, Cambridge CB2 3QZ, United Kingdom*

²*Laboratory for Solid State Physics, ETH Zurich, Schafmattstrasse 16, CH-8093, Zurich, Switzerland*

(Dated: November 10, 2018)

We report the successful imaging of flux vortices in single crystal MgB₂ using transmission electron microscopy. The specimen was thinned to electron transparency (350 nm thickness) by focussed ion beam milling. An artefact of the thinning process was the production of longitudinal thickness undulations of height 1–2 nm in the sample which acted as pinning sites due to the energy required for the vortices to cross them. These had a profound effect on the patterns of vortex order observed which we examine here.

Keywords: MgB₂, Flux vortices, Lorentz microscopy, Superconductivity

I. INTRODUCTION

Superconductors have zero electrical resistance and expel magnetic flux from their interiors (the Meissner effect). If a magnetic field is applied to an ideal (type I) superconductor, no flux enters unless the field exceeds the critical field, H_c , at which the material ceases to be superconducting. However, in type II superconductors, the whole superconducting state is not destroyed at once but above the lower critical field, H_{c1} , magnetic flux penetrates the superconductor by flowing along channels called flux vortices. The vortices consist of a core where superconductivity is suppressed with a size given by the coherence length, ξ , surrounded by circulating supercurrents which persist over a distance called the penetration depth, Λ . The magnetic flux associated with the vortex persists over the same distance. Each vortex carries a single quantum of magnetic flux given by $\Phi_0 = h/2e$ where h is Planck's constant and e is the electron charge. Vortices repel one another and in a defect-free, isotropic superconductor will form a 2-dimensional hexagonal lattice called an Abrikosov lattice¹.

MgB₂ is a superconductor discovered in 2001² with a transition temperature $T_c = 39$ K. It has a hexagonal crystal structure (space group 191: $P6/mmm$) with $a = b = 3.086$ Å and $c = 3.542$ Å with alternating layers of magnesium and boron. There is disagreement in the literature on the values of Λ and ξ at zero temperature and field with ξ_{ab} ranging from 5–13 nm and Λ_{ab} ranging from 48–130 nm^{3–5}. The values in the c direction are less well reported but Moshchalkov *et al.*³ give $\xi_c = 51$ nm and $\Lambda_c = 33.6$ nm. It is an unusual superconductor as it has two types of electronic bonding: σ -bonding from the boron p_{xy} orbitals and π -bonding from the boron p_z orbitals⁴, which give rise to two superconducting gaps the magnitudes of which vary in the literature with $\Delta_\pi = 1.2$ –3.7 meV and $\Delta_\sigma = 6.4$ –7.2 meV⁶.

Flux vortices can be imaged using transmission electron microscopy⁷ due to the magnetic field from the vortices deflecting the electron beam and appear as black-white features in an out-of-focus image (see Fig. 1(a)).

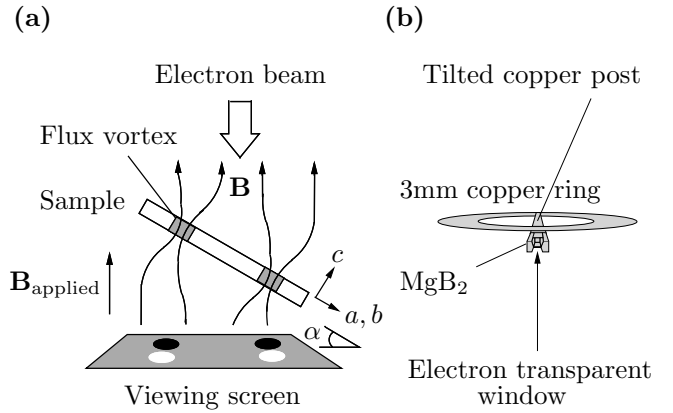


FIG. 1. (a) Experimental arrangement for imaging flux vortices. The electrons are deflected by the component of the B-field from the vortices normal to the electron beam giving a black-white feature in an out-of-focus image. (b) The specimen geometry. The MgB₂ specimen was mounted to a copper post glued to a standard 3 mm diameter copper ring at an angle of 45°. An electron transparent window was then cut by focussed ion-beam milling.

This is a unique imaging technique as it gives information on the internal structure of the vortices, not just the stray fields, and allows imaging at video rate. In this paper, we study the ordering of flux vortices in MgB₂ using this technique and will report on the internal magnetic structure of the vortices and their dynamics in subsequent publications.

II. SAMPLE PREPARATION AND EXPERIMENTAL METHODS

MgB₂ single crystals were synthesised by Dr J. Karpinski as described in ref.⁸ and were thinned to 250 nm in the c direction using focussed ion-beam (FIB) milling so that they were electron transparent. The sample needs to be tilted to a high angle (α in Fig. 1(a)) to max-

imise the electron beam deflection and so was attached to a tilted copper post as illustrated in Fig. 1(b) giving a tilt angle of $\alpha = 45 \pm 1^\circ$ and a projected thickness of 350 nm parallel to the electron beam. A liquid-helium cooled specimen stage was used to cool the sample and energy-filtered images were recorded with a CCD camera using a Philips CM300 transmission electron microscope equipped with a field-emission gun operated at 300 kV. A magnetic field was applied to the sample by altering the setting of the twin lens in the microscope. Further details are given in supp. info. 1.

III. RESULTS AND DISCUSSION

Fig. 2 shows images of flux vortices in MgB_2 taken at 10.8 K in different magnetic fields. The B-fields quoted are calculated from the vortex density averaged across the electron-transparent window. Energy-filtered imaging was used to produce a thickness map of the specimen (see supp. info. 1) showing that the specimen had a thickness parallel to the electron beam of 100 nm at the edge nearest the vacuum which gradually increased to 370 nm in the centre and then fell back to 330 nm at the top-left of the image due to a slight undercutting during FIB milling. The images have been ‘tilt-compensated’ to correct for the apparent compression of the vortex spacings due to the specimen tilt as described in ref.⁹ and the originals are in supp. info. 2.

An unintended effect of the FIB milling was to produce longitudinal thickness undulations running parallel to the ion beam which appear as lines running from top-left to bottom-right of the images in Fig. 2. The thickness map showed that the undulations were 1–2 nm in height and that the dark strip near the bottom-left was 20 nm in height. Interestingly, these act as pinning sites as a vortex needs to become longer to move onto a thicker part of the undulation.

In supp. info. 3 we estimate that it requires ~ 0.5 eV to increase the length of a vortex line by 1 nm in MgB_2 and that the energy cost in moving a vortex from its equilibrium position in an ideal Abrikosov lattice is of a similar magnitude for the displacements we see here indicating that the vortex arrangement is a competition between these two energies. In contrast, the thermal energy of the vortices, $k_B T = 0.0009$ eV, is much lower.

The sequence in Fig. 2 begins at 76.9 G and the field is reduced in subsequent images. Antivortices are seen when the field goes negative as indicated by the reversal of the black-white contrast. To assess the ordering of the vortices, autocorrelation functions of the vortex positions, found by motif matching⁹, are shown to the right of each image. Histograms showing the distribution of vortex spacings and the angle which lines connecting neighbouring vortices (‘bonds’) make to the horizontal are shown in supp. info. 4.

When the field is taken through zero and goes negative, the antivortices first appear, not at the free edge

as might be expected, but furthest away from this where the electron-transparent window meets the bulk sample. As the magnitude of the field is increased, they travel in lines down certain thickness undulations to reach the rest of the sample. The phenomenon of a vortex-free region near the sample edge has been noted by Olsen *et al.*¹⁰ who use magneto-optical imaging to visualise vortices in NbSe_2 and find that a vortex-free region of width 5 μm is seen at the sample edge in an applied field of 2 Oe. The vortex-free region is much larger than the penetration depth (265 nm in NbSe_2) and is ascribed to the vortices forming at the sample edge and then immediately being pushed into the specimen interior by the Lorentz force from the B-field which penetrates the superconductor near the edge^{10,11}. As the applied field is increased, new vortices entering the sample are repelled by those which have already accumulated in the interior and so the vortex-free region diminishes as the field is increased as observed both here and in ref.¹⁰. We are currently undertaking dynamic experiments to clarify how exactly the vortices first enter the sample.

All the autocorrelation functions show a streak at 142° anticlockwise from the horizontal indicating a preference for the vortices to align along the thickness undulations. This ‘vortex channelling’ has also been seen using scanning SQUID microscopy for thickness trenches of depth 25–125 nm in amorphous MoGe ¹².

The image for -6.1 G shows strikingly different spacings parallel and perpendicular to the undulations with the histograms in supp. info. 4 showing a peak for spacings between 856–963 nm corresponding to the vortex spacing parallel to the length of the undulation and peaks at 1070–1177 nm and 1284–1391 nm for spacings perpendicular to this. As the field is increased, the vortex spacings parallel and perpendicular to the undulations become the same as shown by the autocorrelation functions in Fig. 2 becoming circular and the histograms of vortex spacings in supp. info. 4 becoming single peaked.

There is an absence of regularly-spaced peaks in the autocorrelation functions in Fig. 2 indicating that the vortices do not form an ordered lattice. However, the autocorrelation for 76.9 G shows weak peaks which occur at angles of 10° , 55° , 107° and 143° in its inner ring (Supp. Info. 5). These are approximately 45° apart, indicating a tendency towards a square lattice with two different ‘grains’ oriented at 45° to one another rather than the hexagonal Abrikosov lattice expected in the absence of pinning. The histogram of bond directions in Supp. Info. 4 indicates there is a similar fraction of each grain type. Grain boundaries can be seen between different types of vortex order in the image; sometimes these resemble sharp stacking faults but there are also arcs of vortices which give a gradual change in orientation. The order within each grain does not seem to be very good as an exponential decay fit to the peaks of correlation function yields a correlation length of 1.1 vortex spacings.

IV. CONCLUSIONS

We have successfully imaged flux vortices in single crystal MgB_2 using transmission electron microscopy. The ion-thinning process used to thin the sample to electron transparency (350 nm thickness) produced longitudinal thickness undulations 1–2 nm in height creating a pinning landscape which profoundly affected the movement of the vortices and the arrangements they adopted. As the applied magnetic field was increased from zero, flux vortices first appeared in the part of the electron transparent window furthest from the specimen edge. This is probably due to the vortices forming on the specimen edge and then being pushed into the interior by the Lorentz force from the B-field which penetrates near the edge as described in ref.¹⁰. As the field was further in-

creased, the vortices moved along the length of the thickness undulations to reach the rest of the sample. The vortices tended to align in rows along the thickness undulations but no well-ordered lattice was observed at the B-fields used here (0–76.9 G). However, at the highest field of 76.9 G, autocorrelation functions of the vortex positions showed a tendency for the vortices to form a square lattice rather than the hexagonal Abrikosov lattice expected in the absence of pinning.

ACKNOWLEDGMENTS

This work was funded by the Royal Society and the EPSRC, grant number EP/E027903/1.

* Now at Halcyon Molecular, 505 Penobscot Drive, Redwood City, CA 94063, USA.

¹ A. A. Abrikosov, Sov. Phys. JETP **5**, 1174 (1957) Abrik57.

² J. Nagamatsu, N. Nakagawa, T. Muranaka, Y. Zenitani, and J. Akimitsu, Nature **410**, 63 (2001).

³ V. Moshchalkov, M. Menghini, T. Nishio, Q. H. Chen, A. V. Silhanek, V. H. Dao, L. Chibotaru, N. Zhigadlo, and J. Karpinski, Phys. Rev. Lett. **102**, 117001 (2009).

⁴ R. Cubitt, M. R. Eskildsen, C. D. Dewhurst, J. Jun, S. M. Kazakov, and J. Karpinski, Phys. Rev. Lett. **91**, 047002 (2003).

⁵ F. Manzano, A. Carrington, N. E. Hussey, S. Lee, A. Yamamoto, and S. Tajima, Phys. Rev. Lett. **88**, 047002 (2002).

⁶ E. H. Brandt and M. P. Das, J. Supercond. Nov. Magn. **24**, 57 (2011).

⁷ K. Harada, T. Matsuda, J. Bonevich, M. Igarashi, S. Kondo, G. Pozzi, U. Kawabe, and A. Tonomura, Nature **360**, 51 (1992).

⁸ J. Karpinski, S. M. Kazakov, J. Jun, M. Angst, R. Puzniak, A. Wisniewski, and P. Bordet, Physica C **385**, 42 (2003).

⁹ J. C. Loudon and P. A. Midgley, Ultramicroscopy **109**, 700 (2009).

¹⁰ A. A. F. Olsen, H. Hauglin, T. H. Johansen, P. E. Goa, and D. Shantsev, Physica C **408–410**, 537 (2004).

¹¹ M. Marchevsky, L. A. Gurevich, P. H. Kes, and J. Aarts, Phys. Rev. Lett. **75**, 2400 (1995).

¹² B. L. T. Ploure, D. J. V. Harlingen, N. Saha, R. Besseling, M. B. S. Hesselberth, and P. Kes, Phys. Rev. B **66**, 054529 (2002).

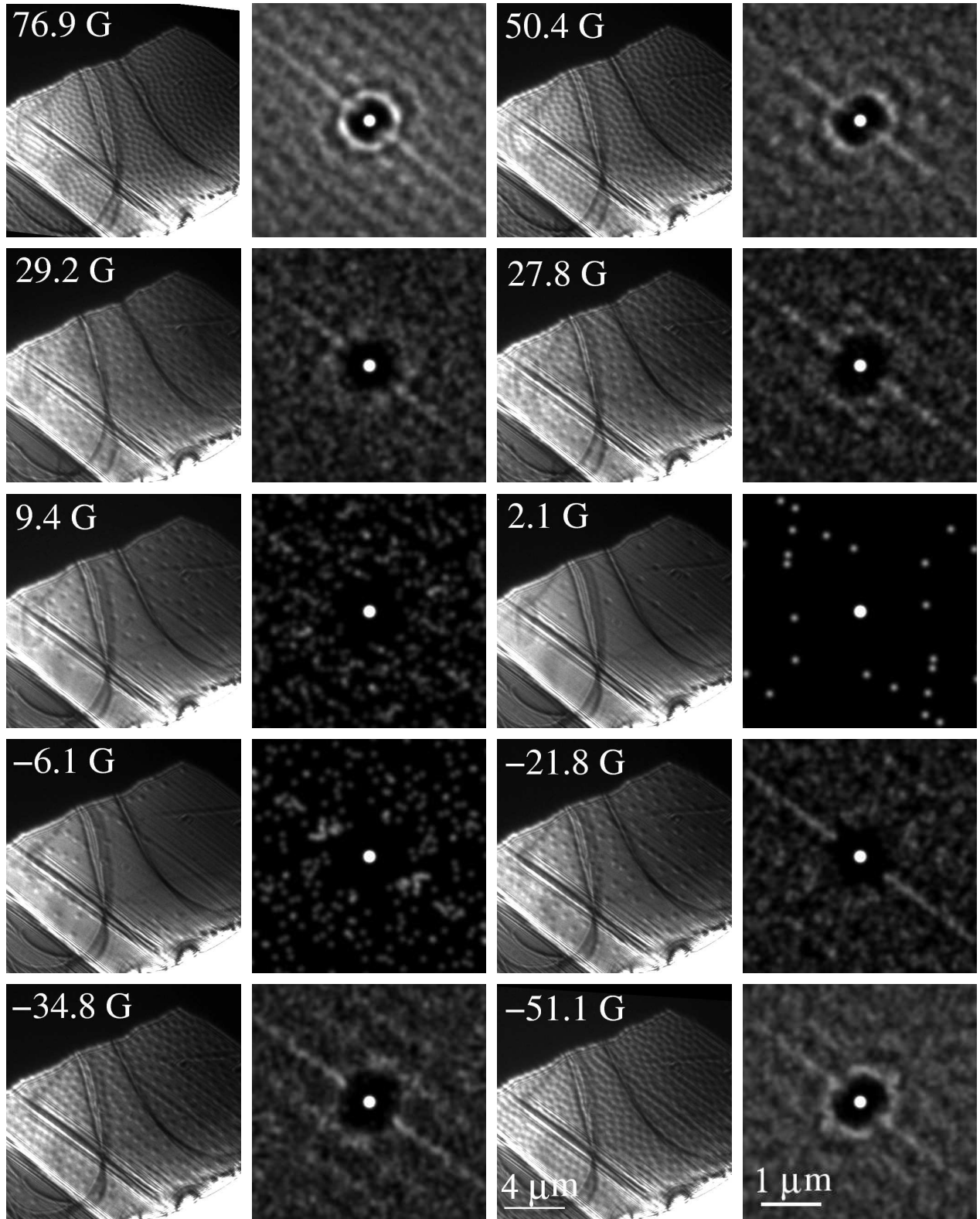


FIG. 2. Sequence of tilt-compensated images showing flux vortices in MgB₂ taken at 10.8 K with a defocus of 3.46 ± 0.02 cm at different B-fields (indicated on the images). The edge of the specimen is at the bottom-right of the image with vacuum beyond. The black area at the top-left is the bulk MgB₂ crystal to which the electron transparent window is attached. The autocorrelation function of the vortex positions is shown to the right of each image.